

The Regularizing Power of Language-Training Deepfake Detectors

Benedikt Hopf, Zongwei Wu, and Radu Timofte

Computer Vision Lab, CAIDAS, University of Würzburg, Germany
{firstname}.{lastname}@uni-wuerzburg.de

Abstract. Recently, thanks to the advent of Multimodal-LLMs, deepfake detectors are striving not only to be generalizable but also interpretable. We propose that these two challenges can effectively be tackled jointly, since describable artifacts typically generalize better, opening the possibility to use language as a regularization mechanism. Since deepfake detection generally suffers from overfitting to low-level domain-specific artifacts, our intuition is that an LLM that has been pretrained on language would prefer high-level artifacts that can be described better. This way, we can use high-level features where possible, while training the model to use low-level features where necessary. We utilize a dual-encoder architecture, pairing a frozen specialist detector with a LoRA-tuned MLLM encoder, and a two-stage training curriculum: first, a binary alignment phase demonstrates that the intrinsic capability of MLLMs can effectively combine features to mitigate overfitting to dataset-specific artifacts. To further bolster generalization and achieve interpretability, we employ a reinforcement learning stage that encourages the model to generate descriptive reasoning before classifying, using only binary labels. By rewarding this “explain-then-classify” behavior, we explicitly incentivize the model to prioritize high-level, robust features. Crucially, this process yields both interpretable descriptions and a further boost in cross-dataset performance, even when reasoning chains are omitted at inference. Extensive experiments on benchmark datasets validate our approach, outperforming state-of-the-art methods by a large margin.

Keywords: Deepfake detection · Regularization · Multimodal reasoning

1 Introduction

With the impressive progress of generative methods [9, 30, 32, 47, 54, 55], deepfake detection, despite being a binary classification task, has become an increasingly critical research topic due to its significant social relevance [6, 59]. Early detectors [1, 29, 48] achieved strong performance on their training distributions thanks to end-to-end learning, but failed to generalize to unseen manipulations. With the advent of multiple datasets [13, 14, 36, 48, 66], the cross-dataset evaluation protocol [4, 23, 34, 42, 50, 64, 67] has become the standard benchmark, emphasizing generalization over mere in-distribution accuracy.

Advances in multimodal large language models (MLLMs) have inspired explainable deepfake detection [19, 51, 69, 70], where language output is leveraged to improve interpretability. We hypothesize that language training can improve generalization by leading to high-level, describable features that vary less between datasets than low-level artifacts. However, this requires an architecture that handles detection and explanation jointly. A common paradigm [19, 51, 69] trains a binary visual detector, optionally with auxiliary cues such as anomaly masks, and feeds the outputs to an MLLM for a *post-hoc* explanation. While improving interpretability, these methods suffer from two limitations: (1) reliance on sub-optimal textual supervision, either handcrafted [51, 69] or human-annotated [19, 70], which limits scalability and cross-dataset adaptability; (2) the classification is performed *before* the MLLM, which merely explains the decision without actively participating in reasoning, thereby missing the opportunity to profit from the MLLM’s language capabilities.

In this work, we propose a joint solution to both problems (Fig. 1) by building a model that learns language descriptions without annotations, while simultaneously improving generalization. To achieve this, we leverage the intrinsic cross-modal alignment of MLLMs to combine features from a specialized detector and a general-purpose vision encoder. This dual-encoder design immediately provides frozen deepfake features, mitigating the overfitting in the general vision encoder. Remarkably, this simple integration alone significantly improves cross-dataset generalization and robustness to distribution shifts.

To further enhance generalization and provide explanations, we formulate our objective through reinforcement learning (RL). Conventional chain-of-thought methods [61] require step-by-step annotated rationales, which are impractical and suboptimal for our setting. Instead, we adopt binary correctness as the sole reward signal, aligning naturally with the task and enabling the MLLM to discover descriptive, decision-relevant reasoning patterns. Specifically, during training, the model generates a textual description highlighting potential manipulation artifacts and then predicts the image’s authenticity. The RL encourages descriptions that reliably lead to correct predictions while penalizing misleading or uninformative ones. Technically, we employ group-relative policy optimization [49] to sample multiple candidate explanations per input, which are ranked and rewarded based on correctness. Consequently, the model jointly reasons over

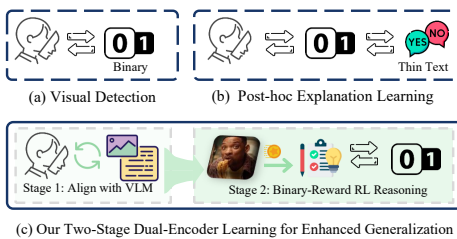


Fig. 1: Motivation. Previous methods usually (a) do not provide language output or (b) learn post-hoc explanations from supervised data (human-annotated or handcrafted features). Using supervised finetuning, reinforcement learning, and a dual-encoder design, our method jointly learns language and detection, leading not only to interpretable descriptions but also benefiting from the implicit regularization of language usage, without requiring annotations.

visual, linguistic, and deepfake-specific features, with this reasoning acting as an implicit regularizer that biases the network toward interpretable and generalizable artifacts rather than spurious correlations. Different from previous CoT in mathematical reasoning, deepfake detection does not profit from intermediary results, but is rather limited by the need to find descriptive artifacts. Still, we show that CoT emerges under RL finetuning, despite not having a positive effect on training accuracy. Therefore, at inference time, we can lift that restriction and proceed without CoT (if we do not explicitly want it for interpretability), leading to a model that prefers descriptive artifacts, but is not restricted to them. This use of reasoning for restricted training has, to the best of our knowledge, not been used before, as it would likely not work well for multi-step mathematics, but only works in cases where overfitting needs to be prevented.

Our main contributions are as follows:

- We propose a unified architecture that leverages the capacity and pretrained knowledge of MLLMs to combine specialized and general features, striking a balance that works well under distribution shifts.
- The finetuning on describable artifacts leads to an internal refinement of features, which further emphasizes generality over dataset-specific artifacts, thereby increasing generalization, even without reasoning at inference time.
- Our model learns language-based explanations from pure binary signals without requiring language annotations.

2 Related Work

While deepfake detectors have progressed from simple general-purpose detectors [48] to more complex ones like frequency-based [21, 37–39, 44], spatial [4, 8, 20, 22, 64, 65, 67, 74], pseudo-fake-based [23, 33, 34, 41, 42, 50, 71] and video-based [31, 68, 72] they still generally only output a single binary label. Recently, the rise of multi-modal large language models has inspired several works [19, 51, 69, 70] to employ language models as supervised deepfake detectors. This can potentially improve interpretability, but supervised training has the problem that ground-truth explanations are generally not available. Therefore, all these methods have their individual downsides, originating mainly from the fact that human annotations are costly and error-prone [51], while hand-crafted heuristics are limited to a fixed number of categories determined by the authors. Furthermore, they treat text as an afterthought instead of fully incorporating it into the main model, missing any regularizing effects it might have.

Related work in general AI-generated content detection has also explored the use of language through annotated datasets [26, 73]. In particular some related works use GRPO [11, 49] to obtain chain-of-thought [61] descriptions. While [25, 27, 28, 52] still require language annotations and are therefore not applicable to every dataset, [35] can – similarly to our method – be used without language annotations. However, their model is not built for partially fake images, ruling it out for deepfakes, which are, in many cases, partial face swaps. Furthermore, they

rely on retrieval augmentation, which provides limited detection performance compared to our dual-encoder design.

3 Preliminaries

This section provides a brief overview of techniques we use to supervise language without ground-truth descriptions.

3.1 Causal Attention

To avoid hallucinations, we need to generate the answer after the description due to the causal structure of language output. In causal language modelling, earlier tokens influence later ones, but not the other way around [56]. More formally:

$$p(o|x, t) = \prod_{n=1}^N p(o_n|x, t, o_{<n}) \quad (1)$$

for input tokens t , image x and output o of length N . Therefore, if the decision is provided first, the explanation is conditioned on the decision, which can lead to hallucination. Therefore, the explanation needs to be provided *first* and the decision needs to be taken *afterwards*.

3.2 Group-Relative Policy Optimization (GRPO)

We use group-relative policy optimization [49] as the reinforcement learning algorithm of our choice, as it is comparably lightweight. We sample a group of G possible answers and calculate a reward r_g , $g \in \{1, \dots, G\} =: \mathcal{G}$ for each answer. Given a group of rewards, we normalize to obtain the advantage A_g as in [11]:

$$A_g = \frac{r_g - \text{mean}_g(r)}{\text{std}_g(r)} \quad (2)$$

setting $A_g = 0 \forall g \in \mathcal{G}$ if $r_i = r_j \forall i, j \in \mathcal{G}$.

To save on VRAM, we use $\pi_{\theta_{old}}(\cdot) = \text{sg}(\pi_{\theta}(\cdot))$, where sg is the stop-gradient operator, avoiding the need to keep an old model in memory. This is a special case of the original algorithm, which includes updating the policy model. Our version is equivalent to a full update at every step, with the added advantage of reducing VRAM consumption. The main loss term then becomes

$$\mathcal{L}_{RL} = -\frac{1}{G} \sum_{g=1}^G \min \left(\frac{\pi_{\theta}(o_g|q)}{\text{sg}(\pi_{\theta}(o_g|q))} \cdot A_g, \text{clip} \left(\frac{\pi_{\theta}(o_g|q)}{\text{sg}(\pi_{\theta}(o_g|q))}, 1 \pm \varepsilon \right) \cdot A_g \right) \quad (3)$$

for group size G , and clipping range $\varepsilon = 0.2$ following [11]. Therefore, answers with larger rewards are encouraged, and ones with smaller rewards (*i.e.* negative advantages) are discouraged. The final loss is then given by

$$\mathcal{L} = \mathcal{L}_{RL} + \beta \cdot \mathcal{L}_{reg} \quad (4)$$

where β is a hyperparameter, and \mathcal{L}_{reg} is the KL-divergence based regularization term as in [49].

4 Method

The fundamental challenge in deepfake detection is learning features that generalize well under distribution shifts, as in-dataset performance can generally easily achieve strong levels. Our central hypothesis is that a combination of general and specific features can limit overfitting. To achieve that, we provide an MLLM with specialized features from a pretrained deepfake detector as well as features from a general vision encoder. We then obtain the decision from the output of the MLLM, rather than a separate classification head, to use the MLLM’s pretrained knowledge to judge how to combine features. While this approach works well under binary pretraining, we then show how forcing explanations from the model using RL can further improve the learnt representations, while simultaneously enabling explainability on datasets with no language annotations.

4.1 Binary Output from Causal LM

Since we intend to avoid separate heads and obtain all answers directly from the LLM’s output, we need to be able to access all common metrics from it. Previous non-language deepfake detectors generally provide scalar output, which allows for calculating all well-known binary metrics such as accuracy, area under the curve (AUC), *etc.* For MLLMs, the output is non-scalar but high-dimensional (and a *yes / no* answer is not continuous). Previous methods [19, 51, 69] have avoided that problem by having a separate classification head. This, however, has the downside that the decision is taken *without* the MLLM, so that its additional capacity and pretrained knowledge cannot be used in classification. We choose a different strategy, which is simple yet effective, obtaining binary output *directly from the MLLM*. In the prompt, we provide the model with a certain output structure and define keywords that should appear depending on the decision (*yes* and *no* in our case). After the model generation, we locate the keyword given the required structure, get the logits for the corresponding two choices, and apply a softmax function to the binary decision.

4.2 Model Architecture

To enable the LLM to combine specific and general features, we use a dual-encoder design and obtain the output directly from the LLM. An overview of the architecture can be seen in Fig. 2. By not using a separate classification head for binary decisions, we involve the LLM even in binary decisions.

We use two vision encoders: a pretrained deepfake detector D as a specialized feature extractor and a vision-language model L with vision-encoder V . We refer to the detector’s last hidden state for some image x as $D(x) \in \mathbb{R}^{n_D \times c_D}$, where n_D and c_D are the number of patches and channel dimension of the latent space of D . The same holds for $V(x) \in \mathbb{R}^{n_V \times c_V}$. The language model outputs logits $y = L(t_1, t_2, \dots, t_n) \in \mathbb{R}^{n_L \times c_L}$ for input tokens $t \in \mathbb{R}^{n \times c_V}$ generated by T from some input string s . Since in general $c_D \neq c_V$, we apply an affine transformation $f : \mathbb{R}^{c_D} \rightarrow \mathbb{R}^{c_V}$, aligning feature dimensions. This allows us to concatenate the

deepfake, general vision, and language features. The entire forward pass can therefore be written as

$$y(s, x) = L(f(D(x)), V(x), T(s)) \quad (5)$$

We keep D pretrained and frozen and only train the adapter layer f . Furthermore, all linear layers in L and V are finetuned using quantized low-rank adaptation [12, 24] in order to keep memory requirements under control.

4.3 Supervised Finetuning (SFT)

This first step is intended to create a unified representation from deepfake features, general vision features, and language. At this point, we just perform binary classification, as this is the only output we can directly supervise. The prompt is always the same, asking for a one-word answer if the shown image is a deepfake. Here we can use SFT, as we know the full answer (*yes* or *no*), since there is no description. We use the standard cross-entropy loss, as is common in fully supervised training. This training step is comparably lightweight, as it is not autoregressive and only requires one generation per image. At the end of that step, the model has a unified internal representation, combining specialized and general features.

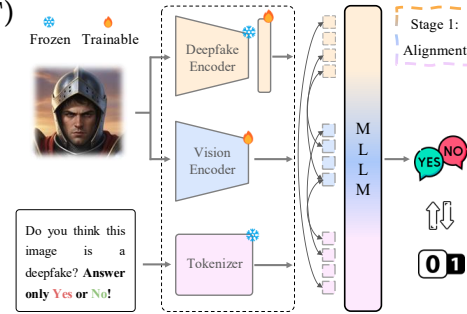


Fig. 2: First stage: modality alignment. Tokens from deepfake detector, vision encoder, and text are passed to the model, asking for a one-word answer. The model outputs a probability distribution over all words, which we can supervise with binary labels and calculate binary metrics from. Note that, unlike previous work, we do not need a separate classification head and directly use the MLLM for classification, improving detection performance and aligning modalities.

4.4 Reinforcement Learning for Feature-Refinement

An overview of the RL pipeline is provided in Fig. 3. Following the example of [11], we use a format reward and a correctness reward. For the format reward r_g^f of group item $g \in \mathcal{G}$ we simply define

$$r_g^f = \begin{cases} 1 & \text{if } s_g \text{ matches } R \\ 0 & \text{else} \end{cases} \quad (6)$$

for sample string s_g and regular expression R as defined in Eq. (7).

$$\langle \text{think} \rangle . * \langle / \text{think} \rangle \backslash \text{n} \langle \text{answer} \rangle [\text{a-z}] + \langle / \text{answer} \rangle \quad (7)$$

The correctness reward r_g^c for the predicted fake probability p_g and correct label l is given as

$$r_g^c = \begin{cases} 1 - |l - p_g| & \text{if } s_g \text{ ends with } \langle / \text{answer} \rangle \\ -1 & \text{else} \end{cases} \quad (8)$$

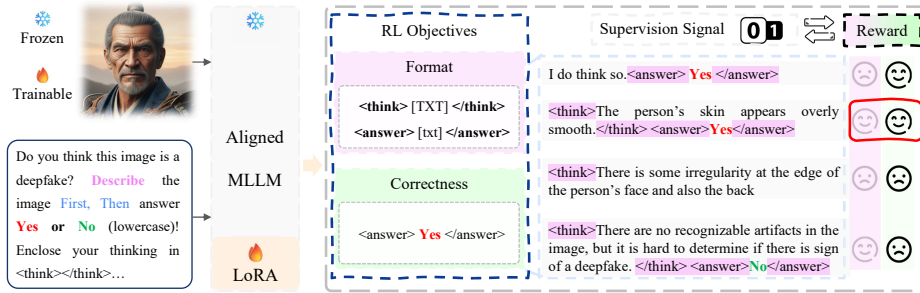


Fig. 3: Second stage: Reinforcement learning. We provide the model with the requested output structure, a question regarding the authenticity of the candidate image, and the image itself. We then sample multiple answers, judge them using our reward functions, and train using GRPO [49]. Negative advantages are discouraged, positive ones encouraged. This strengthens the alignment between the modalities, as all components need to be jointly used in order to generate a cohesive description and decision. Furthermore, it biases the network towards describable artifacts.

From the individual rewards, we calculate a combined final reward $r_g = r_g^f + \alpha \cdot r_g^c$, where α is a hyperparameter.

We find that using r^c before $r^f \approx 1$ causes instability and failure to follow the format. We therefore set $\alpha = 0.01 \ll 1$, such that $A \approx A^f$ unless $r_g^f = r_{g'}^f, \forall g, g' \in \mathcal{G}$, in which case, normalization rescales r^c to have the same magnitude, regardless of the choice of α .

Since L and V have originally been trained together, L can describe features of V . However, D has only been aligned for binary decisions, so L does not inherently know what features from D “mean”. For example, which feature of D refers to a blending boundary vs. a color shift, so long as they both indicate a deepfake. Therefore, the explanation needs to be based on V . Since the final decision is conditional on the explanation (Eq. (1)), the explanation will get gradients from the decision, which is the only part of the output we can supervise. This also leads to a preference for general features when possible, as they are more readily available, thereby improving generalization. Reinforcement learning encourages explanations, which lead to the right decisions, while discouraging ones, which cause wrong decisions. Therefore, if the explanation (by chance) aligns with the features of D , this connection will be strengthened, whereas if they do not, it will be weakened, such that features of D can also be used, if they are needed.

4.5 Inference Modes

Given the two training stages (binary pretraining and RL finetuning), our model can operate in two modes: One-word answer and explanation-based. While we obviously need to choose the latter for explainability, for pure binary decisions, we have a choice. Contrary to mathematical CoT reasoning, deepfake detection is not inherently a multi-step process, so we find reasoning at inference time

to not be necessary and, in fact, detrimental for two reasons: 1. Computational demand: Reasoning requires multiple forward passes, while binary answers can be produced in one step. 2. Logit-quality: Ideally, we do not only want a true binary decision, but also the associated probability (especially important for AUC). If the answer is conditional on an explanation, the final answer’s probability is almost always pretty certain (*i.e.* approximately 100% or 0%), losing the ability to provide meaningful intermediate answers. We therefore perform quantitative experiments in binary mode. In a traditional multi-step reasoning application, this would negate any advantage of reasoning, as it is not used at runtime. However, deepfake detection is a task that is fundamentally limited by overfitting, not by capacity. Therefore, reasoning at training time helps align the model’s features in a generalizable way, which also improves generalization performance during binary inference, acting as a kind of pretext task. This use of reasoning for training-time regularization has, to the best of our knowledge, not been studied before.

5 Experiments

We provide both quantitative and qualitative results, comparing on various benchmark datasets and to language-based and binary detectors.

5.1 Experimental Settings

Datasets. We perform our experiments in the framework of *DeepfakeBench* [63], aligning with their evaluation protocol. We mainly use the recently proposed dataset suite DF40 [66], because it contains the three main fake types: face-swaps (FS), face-reenactment (FR), and entire-face synthesis (EFS), including very recent methods (40 in total). Furthermore, the benchmark is built on two different data sources, enabling cross-dataset testing for very flexible evaluations. We also include some results on the following older datasets: FaceForensics++ (FF++) [48], Celeb-DF-v2 (CDFv2) [36], DFDC [13], and DFDCP [14]. These use much older methods, and, for example, do not include EFS images. However, they have been extensively used in the literature, so we provide results for completeness. Finally, we provide results on SID-Set [26], a fully-synthetic general-object deepfake detection dataset. This allows us to evaluate our model on a very modern dataset and compare to RAIDX [35], which also uses GRPO.

Methods. Due to DF40’s recency, most methods have not evaluated on this setup. We therefore choose methods, that can be trained on DF40, ranging from baselines to recent SOTAs: Xception [7, 48], UIA-ViT [74], CLIP-L [45, 66], and Effort [65]. Furthermore, we compare to state-of-the-art language-based deepfake detectors: BLIP-TI [70], UCLVLM [69], VL-FFD [51] and M2F2 [19], using their provided numbers on CDFv2, DFDC and DFDCP. More comparisons are provided in the supplementary. For SID-Set [26] we compare to LNP [3], AntifakePraompt [5], SIDA [26] and RAIDX [35].

Table 1: Comparison to the state-of-the-art on DF40. Best values are highlighted in **bold**, second best values are underlined. In particular note, the improvement on EFS and in general in terms of accuracy.

in %	Model	Xception	UIA-ViT	(DF40) CLIP-L	Effort	Ours
		ICCV'19 [48]	ECCV'22 [74]	NeurIPS'24 [66]	ICML'25 [65]	
FS (cdf)	ACC↑	<u>77.86</u>	76.21	76.44	76.40	87.77
	AUC↑	76.23	87.57	94.23	90.78	<u>93.43</u>
	AP↑	88.91	95.24	95.36	<u>96.18</u>	97.62
FR (cdf)	ACC↑	<u>79.70</u>	78.13	78.55	78.61	85.70
	AUC↑	83.05	89.22	<u>89.57</u>	81.76	92.38
	AP↑	94.00	<u>95.87</u>	95.36	93.47	97.73
EFS (cdf)	ACC↑	<u>83.43</u>	82.98	82.68	82.49	92.18
	AUC↑	68.04	82.10	85.76	78.85	96.04
	AP↑	89.15	95.28	<u>95.66</u>	94.26	99.12
average	ACC↑	<u>80.33</u>	79.11	79.22	79.17	88.55
	AUC↑	75.78	86.30	<u>89.85</u>	83.80	93.95
	AP↑	90.68	<u>95.46</u>	95.46	94.64	98.16
	ECE↓	<u>18.89</u>	19.95	20.79	20.85	4.07

Metrics. Aligning with the common evaluation protocol [19, 51, 63, 65, 66, 69, 70, 74], we mainly report the area under the receiver-operating characteristic curve (AUC) and additionally accuracy, average precision, F1 and ECE [35, 42, 48].

Implementation Details. We implement our model in the framework of [63], using their data preprocessing, metric calculation, *etc.*, allowing us to restrict improvements to the actual model architecture and training scheme, rather than spurious changes from different sources. We use Qwen2.5-VL-7B [2] as our MLLM and CLIP-L [66] as the deepfake detector.

Computational Requirements. We train our model on Nvidia L40 GPUs (48 GB VRAM). For supervised training, we use a single GPU and a batch size of 4, with training taking less than 24h. For RL, we can only use a per-GPU batch size of 1. We therefore generally use 3 GPUs in parallel. Given the SFT pretraining, training is relatively fast, with most runs converging in less than 24h.

5.2 Comparison to SOTA

Evaluation on DF40. Here, we train on the full training split of DF40 [66], which is based on real images from FF++ [48]. Evaluation is then performed cross-domain on images based on CDF [36]. This setting is particularly hard, as it requires cross-dataset generalization.

Our approach improves generalization compared to the state-of-the-art (*cf.* Tab. 1), beating the previous SOTA CLIP-L [66] by 4.1% AUC. We also see improvements on accuracy and average precision on average over the different fake categories. We observe a particularly large improvement of 9.16% on accuracy, indicating that our method is naturally better calibrated than the state-of-the-

Table 2: Comparison on legacy datasets. Best values are highlighted in **bold**, second best values are underlined. Our model outperforms previous language-based deepfake detectors on average on these datasets.

Model	CDFv2 [36]	DFDCP [14]	DFDC [13]
BLIP-TI-SBI [50, 70]	93.98%	-	-
VL-FFD [51]	84.80%	84.74%	-
UCLVLM [69]	94.71%	91.81%	<u>79.12%</u>
M2F2 [19]	95.10%	87.80%	-
Ours	95.75%	<u>90.29%</u>	82.75%

art, which is confirmed by the expected calibration error (ECE) of 4% compared to about 20% for previous work. When looking at different types of fakes, it stands out that our method performs particularly well on fully synthetic images (+10.28% AUC). We attribute this to the particularly strong risk of overfitting to low-level artifacts in these kinds of images compared to *e.g.* face-swaps [60].

Evaluation on Legacy Datasets. For comparison with other language-based deepfake detectors, we train on the FaceForensics++ [48] dataset and evaluate on CDFv2 [36], DFDC [13], and DFDCP [14], following the established cross-dataset protocol [19, 51, 69]. Since these datasets are no longer the current state-of-the-art, as they only include older methods and, *e.g.*, no fully synthetic images, we note that this serves only as a comparison with models that cannot be trained on DF40, but has limited practical implications, as it has been shown, that performance on these datasets does not generalize well to more modern fakes [66].

Tab. 2 shows that our model outperforms all other language-based deepfake detectors on the most common CDFv2 dataset, as well as the particularly challenging DFDC dataset, while achieving second place on DFDCP. This indicates that while our model works particularly well on modern datasets, it still outperforms previous language-based deepfake detectors on old datasets, showing the flexibility of our technique. Qualitative comparisons to these methods are provided in Sec. C in the supplementary.

Evaluation on SID-Set. As an example of a modern state-of-the-art fully-synthetic general image dataset, we train and test on the fully-generated subset of SID-Set [26] (Tab. 3), aligning with the evaluation protocol of RAIDX [35]. The comparison to RAIDX is particularly interesting, as it is the only other work we know of that can create language outputs without language supervision. While we both use RL, our dual-encoder design and binary pretraining prove more effective than RAIDX’s retrieval augmentation. Our model outperforms all previous work, achieving 99%+ on both metrics and splits.

User Study. We performed a user study, comparing some of our explanations to explanations from DD-VQA [70] (human annotations). Users scored explanations on a scale from 1 (bad) to 5 (good) depending on whether the described artifacts exist in the image; details are provided in the supplementary. Our method achieves an average score of 3.57 with a standard deviation of 1.1, compared to

Table 3: Comparison on fully synthetic images. Best values are highlighted in **bold**, second best values are underlined, all values are given in %. Our model outperforms previous methods. In particular, we outperform RAIDX [35], due to our dual-encoder design and binary pretraining.

Model	Venue	Real		Fake		average	
		ACC↑	F1↑	ACC↑	F1↑	ACC↑	F1↑
LNP	arXiv’23 [3]	71.2	83.2	91.8	95.7	81.5	89.5
AntifakePrompt	arXiv’23 [5]	64.8	78.6	93.8	96.8	79.3	87.7
SIDA-13B	CVPR’25 [26]	96.7	97.3	98.7	99.3	97.7	98.3
RAIDX	MM’25 [35]	<u>98.5</u>	<u>98.9</u>	<u>99.4</u>	<u>99.5</u>	<u>99.0</u>	<u>99.2</u>
Ours	-	99.4	99.7	99.6	99.8	99.5	99.7

DD-VQA with 3.83 and a standard deviation of 0.99, indicating that our method performs similarly to human annotations.

Hallucination Analysis. We test for hallucinations by generating reasoning on 40 images, which have annotations from DD-VQA [70], and asking Google’s Gemini to judge if there is any overlap between the explanations, indicating that both answers refer to the same artifact. We find a hallucination rate of only 7.5%, indicating that most of our model’s answers are based on facts. This was expected because otherwise, the reasoning training could not conceivably improve detection performance. We evaluate artifact-level precision rather than exact wording or exhaustive localization: an explanation is counted as useful only when at least one claimed artifact is visibly supported by the image.

To test grounding more directly, we also gave Gemini images along with the explanations and asked for a 0–5 image-match score. Ours obtains 3.61 ± 0.99 vs. DD-VQA 3.79 ± 0.78 . Gemini flagged two partial hallucinations among 20 explanations; both also contained another visible artifact, so we will report them as partial errors rather than fully correct cases. On this 20-explanation claim-level check, Gemini marked 95.7% of our artifact claims as image-supported, close to 96.4% for DD-VQA.

Textual variety. We calculate self-BLEU to check for repetitiveness in our model’s outputs. Here higher numbers indicate more repetitions/similarity between explanations. Our model achieves a self-BLEU value of 0.085, which is considerably lower than the explanations from DD-VQA at 0.214. This shows that our model actually creates individual explanations per input image and does not only reuse the same standard explanation.

Comparison of Computational Demands. Since LLMs are by definition large, our model requires a lot more parameters and compute than non-language deepfake detectors. We utilize the 7B version of Qwen-2.5-VL [2]. This downside is common to all language-output detectors, as they rely on an LLM (*e.g.* M2F2 [19] and UCLVLM [69] also use a 7B model, and VL-FFD [51] even uses a 13B model). Finally, GRPO’s repeated sampling [49] causes image throughput

Table 4: Key component analysis. Stage 1 shows that our dual-encoder design is optimal for generalization due to the combined use of specialized and general features. Dropping either one of the encoders leads to performance loss. Furthermore, we show that RL finetuning in Stage 2 can further improve generalization by explicitly enforcing describable features. However, when relying exclusively or during inference on RL, we observe reduced performance. This confirms our use of RL as only a regularizing step.

	LLM	DF-Enc. [66]	V-Enc.	SFT	RL	RL inf.	avg. AUC
Baseline		✓		✓			89.85%
Ours Stage 1	✓		✓	✓			76.22%
	✓	✓		✓			91.56%
	✓	✓	✓	✓			93.34%
Ours Stage 2	✓	✓	✓		✓		84.47%
	✓	✓	✓	✓	✓	✓	81.63%
	✓	✓	✓	✓	✓		93.95%

during training to be low. However, using our supervised pretraining, we reduce training times to 12-24h by reducing the number of necessary training images.

5.3 Ablation and Discussion

Key Component Analysis. Our ablation study is shown in Tab. 4. Starting from the baseline detector CLIP-L, we see that incorporating the LLM already leads to a performance improvement (+1.7%), likely due to the model’s pretrained internal knowledge. However, adding the vision encoder leads to a further improvement (+1.8%), as the LLM can now create a combined representation and rely on its vision encoder for general features, enhancing generalization performance. In contrast, relying solely on the vision encoder yields significantly lower performance, as the model must learn specialized artifact representations itself, which quickly leads to overfitting. This shows that our dual encoder paradigm is optimal for generalization performance, avoiding overfitting despite the large capacity.

Regarding RL, we find that exclusively relying on it is suboptimal because the weaker learning signal can not sufficiently incorporate both types of features, and relying on it at inference time also reduces performance due to degraded logit quality (see Sec. 4.5). In contrast, when starting from the strong base model of binary pretraining, RL finetuning can refine the learnt representation, providing a regularizing effect and improving performance to the best AUC of 93.95% (+0.61%). This further validates the use of language as a regularization tool, as its explicit enforcement yields improvements beyond the implicit binary baseline.

We therefore see that added capacity can quickly lead to overfitting if it is not avoided by providing frozen specialized features separately. Furthermore, we observe that additional general context improves performance by reducing the focus on specialized features and therefore overfitting. The LLM implicitly performs this alignment; however, explicitly enforcing the use of general features takes the generalization improvement another step forward.

Post-hoc reasoning. We perform an experiment to isolate the effect of generating reasoning during training. Here, we use the same settings, but invert the format (`<answer>...</answer><think>...</think>`), so that causal masking prevents reasoning to influence the decision, while RL is still present. Details are provided in Sec. F. We measure a performance of 92.93%, significantly lower than our correct RL setup and even lower than SFT only. This shows that the actual reasoning (as opposed to *e.g.* RL itself) acts as a regularizer during training.

Shift of features due to RL. To measure if RL actually shifts the model’s internal features away from generator-specific low-level artifacts, we perform an experiment, where we measure the shift in the distribution of features under the change of generator (change of low-level artifacts) and a shift of the underlying data (change of low and high-level features), by the Fréchet distance (using splits of DF40). We calculate the relative change for low-level features as $\frac{\Delta_{generator}}{\Delta_{data}}$. Here, our model gets a value of 0.525 before and 0.479 after RL finetuning. This proxy suggests reduced reliance on generator-specific low-level shifts after RL, consistent with the intuition that high-level features are necessary for description. The prompt is the same as for all evaluations.

Causal grounding. To test image-grounding for the decision, we mark boxes around the artifact named in the explanation, then mask them and compare to a matched face region, symmetric when possible. On $N = 50$ correctly classified examples, we measure the error $(1 - p_y)$ for the true class. Masking the cited artifact region causes a 45% larger error (geometric average) than masking the matched non-cited region, suggesting the explanations identify decision-relevant regions (error is calculated in non-reasoning evaluation mode).

Out-of-Domain Examples. We analyze the explanations and decisions of our model on out-of-domain samples, using exemplary images from popular online deepfakes and state-of-the-art generators [10, 17, 40, 46, 62, 75] (Fig. 4).

Our model can correctly identify the famous deepfake of Will Smith eating spaghetti based on an artifact at the edge of the face. This shows the descriptive quality of our method, despite the distribution shift from the training dataset.

In the top right of Fig. 4, we show a neural plagiarism [75] image. Our detector can recognize the image as fake and provide a reasonable explanation. This shows robustness to distribution shifts even beyond the realm of deepfakes.

The image in the left center is a non-face image, so we use our model trained on the SID-Set [26]. This shows that our method can be applied to general images and will also learn descriptive explanations for non-face fakes.

In the right center, we show a failure case. This image is of particularly high quality and does not show any of the common diffusion artifacts (smooth textures, excessive symmetry, inconsistent lighting, ...). Therefore, our method fails to detect the image as a deepfake. Providing the image to ChatGPT gets the same result. This emphasizes the need for higher-quality datasets that encourage models to learn even more detailed signs.

In the lower left, we show an image of a person with oil on their face. Even under those harder conditions, our model can still identify the image as fake

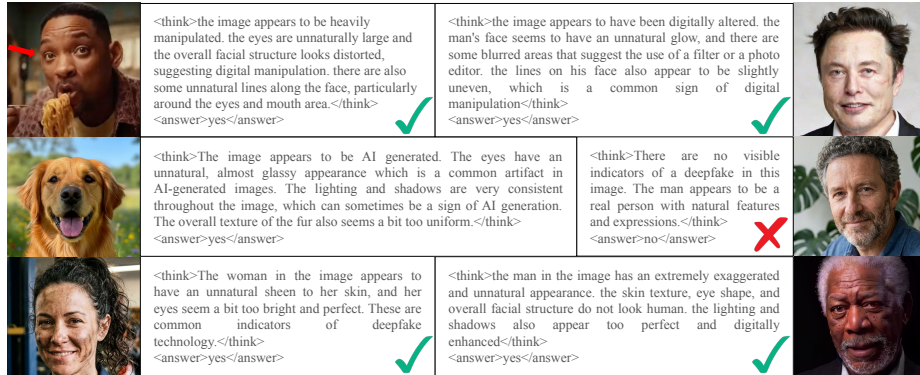


Fig. 4: Out-of-domain examples. The first image is the famous Will-Smith-eating-spaghetti example [62] by Google’s Veo 3 [10], the second one is taken from [75]. The center left is generated by Google Gemini 2.5 Flash [17], the center right and lower left by Gemini 3 Flash [46], and the final image is a still from [40]. We specifically include a failure case, showing that very high-quality images can avoid detection. The red arrow has been manually added by us to aid the viewer in finding the described artifact.

and provide a reasonable explanation. This shows that our model can generalize beyond the bounds of the training dataset.

Finally, on the lower right, we show a famous deepfake of Morgan Freeman. Although it is relatively old (2021), it remains a very high-quality fake. Our model correctly identifies the deepfake, pointing to its “exaggerated and unnatural appearance”. For a human observer, this would likely also be the ground for detection, as the image appears overly sharp and not like a natural photograph. However, of course, such an effect could also be achieved by classical photo editing, without a deep model. More discussions, examples, and comparisons to ChatGPT are provided in the supplementary.

6 Conclusion

This work demonstrates that integrating language reasoning into deepfake detection can provide an overlooked benefit beyond interpretability. We utilize a dual-encoder architecture – pairing a frozen specialist with a general-purpose vision encoder – to effectively balance fine-grained artifacts and global context. Our two-stage training curriculum is key to this synergy: binary pretraining ensures the integration of specialized features, while subsequent RL-based explanation tuning acts as a regularizer to incentivize the use of high-level, semantic cues. This approach leads to significantly improved cross-dataset generalization across multiple benchmarks. Additionally, our method produces a model capable of generating high-quality explanations without requiring any manual language supervision during training. Ultimately, because the gains stem from robust feature selection rather than explicit step-by-step reasoning, these performance advantages persist even when reasoning is omitted at inference time.

References

1. Afchar, D., Nozick, V., Yamagishi, J., Echizen, I.: Mesonet: a compact facial video forgery detection network. 2018 IEEE International Workshop on Information Forensics and Security (WIFS) pp. 1–7 (2018), <https://api.semanticscholar.org/CorpusID:52157475> 1
2. Bai, S., Chen, K., Liu, X., Wang, J., Ge, W., Song, S., Dang, K., Wang, P., Wang, S., Tang, J., Zhong, H., Zhu, Y., Yang, M., Li, Z., Wan, J., Wang, P., Ding, W., Fu, Z., Xu, Y., Ye, J., Zhang, X., Xie, T., Cheng, Z., Zhang, H., Yang, Z., Xu, H., Lin, J.: Qwen2.5-vl technical report (2025), <https://arxiv.org/abs/2502.13923> 9, 11, 4, 5
3. Bi, X., Liu, B., Yang, F., Xiao, B., Li, W., Huang, G., Cosman, P.C.: Detecting generated images by real images only. ArXiv [abs/2311.00962](https://arxiv.org/abs/2311.00962) (2023), <https://api.semanticscholar.org/CorpusID:264935324> 8, 11
4. Cao, J., Ma, C., Yao, T., Chen, S., Ding, S., Yang, X.: End-to-end reconstruction-classification learning for face forgery detection. In: Proceedings of the IEEE/CVF Conference on Computer Vision and Pattern Recognition (CVPR). pp. 4113–4122 (June 2022) 1, 3, 4
5. Chang, Y.M., Yeh, C., Chiu, W.C., Yu, N.: Antifakeprompt: Prompt-tuned vision-language models are fake image detectors. ArXiv [abs/2310.17419](https://arxiv.org/abs/2310.17419) (2023), <https://api.semanticscholar.org/CorpusID:264490490> 8, 11
6. Chen, H., Magramo, K.: Finance worker pays out \$25 million after video call with deepfake “chief financial officer” (Feb 2024), <https://edition.cnn.com/2024/02/04/asia/deepfake-cfo-scam-hong-kong-intl-hnk> 1
7. Chollet, F.: Xception: Deep learning with depthwise separable convolutions. 2017 IEEE Conference on Computer Vision and Pattern Recognition (CVPR) pp. 1800–1807 (2016), <https://api.semanticscholar.org/CorpusID:2375110> 8
8. Cui, X., Li, Y., Zhu, D., Zhou, J., Dong, J., Lyu, S.: Forensics adapter: Unleashing clip for generalizable face forgery detection (2025), <https://arxiv.org/abs/2411.19715> 3
9. Deepfakes: deepfakes_faceswap. <https://github.com/deepfakes/faceswap> (2019) 1
10. Deepmind, G.: Veo: a text-to-video generation system (2025) 13, 14, 2
11. DeepSeek-AI: Deepseek-r1: Incentivizing reasoning capability in llms via reinforcement learning (2025), <https://arxiv.org/abs/2501.12948> 3, 4, 6
12. Dettmers, T., Pagnoni, A., Holtzman, A., Zettlemoyer, L.: Qlora: Efficient finetuning of quantized llms (2023), <https://arxiv.org/abs/2305.14314> 6
13. Dolhansky, B., Bitton, J., Pflaum, B., Lu, J., Howes, R., Wang, M., Canton-Ferrer, C.: The deepfake detection challenge dataset. ArXiv [abs/2006.07397](https://arxiv.org/abs/2006.07397) (2020), <https://api.semanticscholar.org/CorpusID:219687616> 1, 8, 10, 3
14. Dolhansky, B., Howes, R., Pflaum, B., Baram, N., Canton-Ferrer, C.: The deepfake detection challenge (dfdc) preview dataset. ArXiv [abs/1910.08854](https://arxiv.org/abs/1910.08854) (2019), <https://api.semanticscholar.org/CorpusID:204800939> 1, 8, 10, 3
15. Efron, B.: Bootstrap Methods: Another Look at the Jackknife. The Annals of Statistics **7**(1), 1–26 (1979). <https://doi.org/10.1214/aos/1176344552>, <https://doi.org/10.1214/aos/1176344552> 5
16. Favreau, J., Lucas, G.: The mandalorian (2020), <https://www.disneyplus.com/en-de/browse/entity-422f6dcc-226f-44e7-98d4-22de69b31cf3?distributionPartner=google> 1, 2

17. Fortin, A., Vernade, G., Kampf, K., Reshi, A.: Introducing gemini 2.5 flash image, our state-of-the-art image model (2025), <https://developers.googleblog.com/en/introducing-gemini-2-5-flash-image/> 13, 14, 1, 2
18. Guo, X., Liu, X., Ren, Z., Grosz, S., Masi, I., Liu, X.: Hierarchical fine-grained image forgery detection and localization (2023), <https://arxiv.org/abs/2303.17111> 4
19. Guo, X., Song, X., Zhang, Y., Liu, X., Liu, X.: Rethinking vision-language model in face forensics: Multi-modal interpretable forged face detector (2025), <https://arxiv.org/abs/2503.20188> 2, 3, 5, 8, 9, 10, 11, 4, 6
20. Guo, Y., Zhen, C., Yan, P.: Controllable guide-space for generalizable face forgery detection. 2023 IEEE/CVF International Conference on Computer Vision (ICCV) pp. 20761–20770 (2023), <https://api.semanticscholar.org/CorpusID:260164891> 3, 4
21. Hasanaath, A.A., Luqman, H., Katib, R., Anwar, S.: Fsb: Deepfakes detection with frequency enhanced self-blended images. ArXiv [abs/2406.08625](https://arxiv.org/abs/2406.08625) (2024), <https://api.semanticscholar.org/CorpusID:270440586> 3
22. He, Y., Yu, N., Keuper, M., Fritz, M.: Beyond the spectrum: Detecting deepfakes via re-synthesis. ArXiv [abs/2105.14376](https://arxiv.org/abs/2105.14376) (2021), <https://api.semanticscholar.org/CorpusID:235254766> 3
23. Hopf, B., Timofte, R.: Practical manipulation model for robust deepfake detection. In: Proceedings of the IEEE/CVF International Conference on Computer Vision (ICCV) Workshops. pp. 5675–5684 (October 2025) 1, 3, 4, 12
24. Hu, J.E., Shen, Y., Wallis, P., Allen-Zhu, Z., Li, Y., Wang, S., Chen, W.: Lora: Low-rank adaptation of large language models. ArXiv [abs/2106.09685](https://arxiv.org/abs/2106.09685) (2021), <https://api.semanticscholar.org/CorpusID:235458009> 6
25. Huang, T.M., Lin, W.T., Hua, K.L., Cheng, W.H., Yamagishi, J., Chen, J.C.: Thinkfake: Reasoning in multimodal large language models for ai-generated image detection (2025), <https://arxiv.org/abs/2509.19841> 3, 11
26. Huang, Z., Hu, J., Li, X., He, Y., Zhao, X., Peng, B., Wu, B., Huang, X., Cheng, G.: Sida: Social media image deepfake detection, localization and explanation with large multimodal model. 2025 IEEE/CVF Conference on Computer Vision and Pattern Recognition (CVPR) pp. 28831–28841 (2025), <https://api.semanticscholar.org/CorpusID:274515145> 3, 8, 10, 11, 13
27. Huang, Z., Li, T., Li, X., Wen, H., He, Y., Zhang, J., Fei, H., Yang, X., Huang, X., Peng, B., Cheng, G.: So-fake: Benchmarking and explaining social media image forgery detection (2025), <https://arxiv.org/abs/2505.18660> 3, 11
28. Jiang, C., Dong, W., Zhang, Z., Yu, F., Peng, W., Yuan, X., Bi, Y., Zhao, M., Zhou, Z., Si, C., Shan, C.: Ivy-fake: A unified explainable framework and benchmark for image and video aigc detection (2026), <https://arxiv.org/abs/2506.00979> 3, 11
29. Jung, T., Kim, S., Kim, K.: Deepvision: Deepfakes detection using human eye blinking pattern. IEEE Access 8, 83144–83154 (2020), <https://api.semanticscholar.org/CorpusID:218651878> 1
30. Karras, T., Laine, S., Aittala, M., Hellsten, J., Lehtinen, J., Aila, T.: Analyzing and improving the image quality of stylegan. 2020 IEEE/CVF Conference on Computer Vision and Pattern Recognition (CVPR) pp. 8107–8116 (2019), <https://api.semanticscholar.org/CorpusID:209202273> 1
31. Kim, T., Choi, J., Jeong, Y., Noh, H., Yoo, J., Baek, S., Choi, J.: Beyond spatial frequency: Pixel-wise temporal frequency-based deepfake video detection (2025), <https://arxiv.org/abs/2507.02398> 3
32. Kowalski, M.: Faceswap. <https://github.com/MarekKowalski/FaceSwap> (2018) 1, 12

33. Larue, N., Vu, N.S., Struc, V., Peer, P., Christophides, V.: Seeable: Soft discrepancies and bounded contrastive learning for exposing deepfakes. 2023 IEEE/CVF International Conference on Computer Vision (ICCV) pp. 20954–20964 (2022), <https://api.semanticscholar.org/CorpusID:253734417> 3, 4
34. Li, L., Bao, J., Zhang, T., Yang, H., Chen, D., Wen, F., Guo, B.: Face x-ray for more general face forgery detection. 2020 IEEE/CVF Conference on Computer Vision and Pattern Recognition (CVPR) pp. 5000–5009 (2019), <https://api.semanticscholar.org/CorpusID:209516424> 1, 3, 4, 12
35. Li, T., Huang, Z., Wen, H., He, Y., Lyu, S., Wu, B., Cheng, G.: Raidx: A retrieval-augmented generation and grpo reinforcement learning framework for explainable deepfake detection. Proceedings of the 33rd ACM International Conference on Multimedia (2025), <https://api.semanticscholar.org/CorpusID:280536379> 3, 8, 9, 10, 11
36. Li, Y., Yang, X., Sun, P., Qi, H., Lyu, S.: Celeb-df: A large-scale challenging dataset for deepfake forensics. 2020 IEEE/CVF Conference on Computer Vision and Pattern Recognition (CVPR) pp. 3204–3213 (2019), <https://api.semanticscholar.org/CorpusID:212726430> 1, 8, 9, 10, 3
37. Liu, H., Li, X., Zhou, W., Chen, Y., He, Y., Xue, H., Zhang, W., Yu, N.: Spatial-phase shallow learning: Rethinking face forgery detection in frequency domain. 2021 IEEE/CVF Conference on Computer Vision and Pattern Recognition (CVPR) pp. 772–781 (2021), <https://api.semanticscholar.org/CorpusID:232092167> 3, 4
38. Luo, Y., Zhang, Y., Yan, J., Liu, W.: Generalizing face forgery detection with high-frequency features. 2021 IEEE/CVF Conference on Computer Vision and Pattern Recognition (CVPR) pp. 16312–16321 (2021), <https://api.semanticscholar.org/CorpusID:232320599> 3
39. Masi, I., Killekar, A., Mascarenhas, R.M., Gurudatt, S.P., AbdAlmageed, W.: Two-branch recurrent network for isolating deepfakes in videos. ArXiv **abs/2008.03412** (2020), <https://api.semanticscholar.org/CorpusID:221090663> 3
40. Nep, D.: This is not morgan freeman - a deepfake singularity (2021) 13, 14
41. Nguyen, D., Astrid, M., Kacem, A., Ghorbel, E., Aouada, D.: Vulnerability-aware spatio-temporal learning for generalizable deepfake video detection (2025), <https://arxiv.org/abs/2501.01184> 3, 4
42. Nguyen, D., Mejri, N., Singh, I.P., Kuleshova, P., Astrid, M., Kacem, A., Ghorbel, E., Aouada, D.: Laa-net: Localized artifact attention network for quality-agnostic and generalizable deepfake detection. In: Proceedings of the IEEE/CVF Conference on Computer Vision and Pattern Recognition. pp. 17395–17405 (2024) 1, 3, 9, 4, 8, 12
43. OpenAI: Gpt-5.1: A smarter, more conversational chatgpt (Nov 2025), <https://openai.com/index/gpt-5-1/> 1, 2
44. Qian, Y., Yin, G., Sheng, L., Chen, Z., Shao, J.: Thinking in frequency: Face forgery detection by mining frequency-aware clues. ArXiv **abs/2007.09355** (2020), <https://api.semanticscholar.org/CorpusID:220647499> 3
45. Radford, A., Kim, J.W., Hallacy, C., Ramesh, A., Goh, G., Agarwal, S., Sastry, G., Askell, A., Mishkin, P., Clark, J., Krueger, G., Sutskever, I.: Learning transferable visual models from natural language supervision (2021), <https://arxiv.org/abs/2103.00020> 8
46. Raisinghani, N.: Nano banana 2: Combining pro capabilities with lightning-fast speed (Feb 2026), <https://blog.google/innovation-and-ai/technology/ai/nano-banana-2/> 13, 14, 2

47. Rombach, R., Blattmann, A., Lorenz, D., Esser, P., Ommer, B.: High-resolution image synthesis with latent diffusion models (2021) [1](#)
48. Rössler, A., Cozzolino, D., Verdoliva, L., Riess, C., Thies, J., Nießner, M.: Face-Forensics++: Learning to detect manipulated facial images. In: International Conference on Computer Vision (ICCV) (2019) [1](#), [3](#), [8](#), [9](#), [10](#), [4](#), [12](#)
49. Shao, Z., Wang, P., Zhu, Q., Xu, R., Song, J., Bi, X., Zhang, H., Zhang, M., Li, Y.K., Wu, Y., Guo, D.: Deepseekmath: Pushing the limits of mathematical reasoning in open language models (2024), <https://arxiv.org/abs/2402.03300> [2](#), [3](#), [4](#), [7](#), [11](#)
50. Shiohara, K., Yamasaki, T.: Detecting deepfakes with self-blended images. 2022 IEEE/CVF Conference on Computer Vision and Pattern Recognition (CVPR) pp. 18699–18708 (2022), <https://api.semanticscholar.org/CorpusID:248227916> [1](#), [3](#), [10](#), [4](#), [8](#), [12](#)
51. Sun, K., Chen, S., Yao, T., Sun, X., Ding, S., Ji, R.: Towards general visual-linguistic face forgery detection. 2025 IEEE/CVF Conference on Computer Vision and Pattern Recognition (CVPR) pp. 19576–19586 (2023), <https://api.semanticscholar.org/CorpusID:260334219> [2](#), [3](#), [5](#), [8](#), [9](#), [10](#), [11](#), [4](#), [6](#)
52. Tan, H., Lan, J., Tan, Z., Liu, A., Song, C., Shi, S., Zhu, H., Wang, W., Wan, J., Lei, Z.: Veritas: Generalizable deepfake detection via pattern-aware reasoning (2026), <https://arxiv.org/abs/2508.21048> [3](#), [11](#)
53. Tan, M., Le, Q.V.: Efficientnet: Rethinking model scaling for convolutional neural networks. ArXiv [abs/1905.11946](#) (2019), <https://api.semanticscholar.org/CorpusID:167217261> [4](#)
54. Thies, J., Zollhöfer, M., Nießner, M.: Deferred neural rendering. ACM Transactions on Graphics (TOG) **38**, 1 – 12 (2019), <https://api.semanticscholar.org/CorpusID:219950625> [1](#)
55. Thies, J., Zollhöfer, M., Stamminger, M., Theobalt, C., Nießner, M.: Face2face: Real-time face capture and reenactment of rgb videos. 2016 IEEE Conference on Computer Vision and Pattern Recognition (CVPR) pp. 2387–2395 (2016), <https://api.semanticscholar.org/CorpusID:52858569> [1](#)
56. Vaswani, A., Shazeer, N.M., Parmar, N., Uszkoreit, J., Jones, L., Gomez, A.N., Kaiser, L., Polosukhin, I.: Attention is all you need. In: Neural Information Processing Systems (2017), <https://api.semanticscholar.org/CorpusID:13756489> [4](#)
57. Veo: Veo 3 demo | sailor and the sea (2025), <https://www.youtube.com/watch?v=mCFMnOUkRt0> [1](#)
58. Wadhwa, N., Garg, R., Jacobs, D.E., Feldman, B.E., Kanazawa, N., Carroll, R., Movshovitz-Attias, Y., Barron, J.T., Pritch, Y., Levoy, M.: Synthetic depth-of-field with a single-camera mobile phone. ACM Transactions on Graphics **37**(4), 1–13 (Jul 2018). <https://doi.org/10.1145/3197517.3201329>, <http://dx.doi.org/10.1145/3197517.3201329> [11](#)
59. Wakefield, J.: Deepfake presidents used in russia-ukraine war (Mar 2022), <https://www.bbc.com/news/technology-60780142> [1](#)
60. Wang, S.Y., Wang, O., Zhang, R., Owens, A., Efros, A.A.: Cnn-generated images are surprisingly easy to spot. . . for now. 2020 IEEE/CVF Conference on Computer Vision and Pattern Recognition (CVPR) pp. 8692–8701 (2019), <https://api.semanticscholar.org/CorpusID:209444798> [10](#)
61. Wei, J., Wang, X., Schuurmans, D., Bosma, M., Ichter, B., Xia, F., Chi, E., Le, Q., Zhou, D.: Chain-of-thought prompting elicits reasoning in large language models (2023), <https://arxiv.org/abs/2201.11903> [2](#), [3](#)

62. Wikipedia: (Oct 2025), https://en.wikipedia.org/wiki/Will_Smith_Eating_Spaghetti_test 13, 14
63. Yan, Z., Zhang, Y., Yuan, X., Lyu, S., Wu, B.: Deepfakebench: A comprehensive benchmark of deepfake detection. ArXiv **abs/2307.01426** (2023), <https://api.semanticscholar.org/CorpusID:259342157> 8, 9, 4, 12
64. Yan, Z., Luo, Y., Lyu, S., Liu, Q., Wu, B.: Transcending forgery specificity with latent space augmentation for generalizable deepfake detection. 2024 IEEE/CVF Conference on Computer Vision and Pattern Recognition (CVPR) pp. 8984–8994 (2023), <https://api.semanticscholar.org/CorpusID:265294623> 1, 3, 4
65. Yan, Z., Wang, J., Jin, P., Zhang, K.Y., Liu, C., Chen, S., Yao, T., Ding, S., Wu, B., Yuan, L.: Orthogonal subspace decomposition for generalizable ai-generated image detection (2025), <https://arxiv.org/abs/2411.15633> 3, 8, 9, 4
66. Yan, Z., Yao, T., Chen, S., Zhao, Y., Fu, X., Zhu, J., Luo, D., Yuan, L., Wang, C., Ding, S., et al.: Df40: Toward next-generation deepfake detection. arXiv preprint arXiv:2406.13495 (2024) 1, 8, 9, 10, 12, 3
67. Yan, Z., Zhang, Y., Fan, Y., Wu, B.: Ucf: Uncovering common features for generalizable deepfake detection. 2023 IEEE/CVF International Conference on Computer Vision (ICCV) pp. 22355–22366 (2023), <https://api.semanticscholar.org/CorpusID:258352431> 1, 3, 4
68. Yan, Z., Zhao, Y., Chen, S., Guo, M., Fu, X., Yao, T., Ding, S., Yuan, L.: Generalizing deepfake video detection with plug-and-play: Video-level blending and spatiotemporal adapter tuning (2024), <https://arxiv.org/abs/2408.17065> 3
69. Yu, P., Fei, J., Gao, H., Feng, X., Xia, Z., Chang, C.H.: Unlocking the capabilities of large vision-language models for generalizable and explainable deepfake detection (2025), <https://arxiv.org/abs/2503.14853> 2, 3, 5, 8, 9, 10, 11, 4, 6
70. Zhang, Y., Colman, B., Guo, X., Shahriyari, A., Bharaj, G.: Common sense reasoning for deepfake detection (2024), <https://arxiv.org/abs/2402.00126> 2, 3, 8, 9, 10, 11, 4, 5, 7
71. Zhao, T., Xu, X., Xu, M., Ding, H., Xiong, Y., Xia, W.: Learning self-consistency for deepfake detection. 2021 IEEE/CVF International Conference on Computer Vision (ICCV) pp. 15003–15013 (2020), <https://api.semanticscholar.org/CorpusID:236456448> 3
72. Zheng, Y., Bao, J., Chen, D., Zeng, M., Wen, F.: Exploring temporal coherence for more general video face forgery detection (2021), <https://arxiv.org/abs/2108.06693> 3
73. Zhou, Z., Luo, Y., Wu, Y., Sun, K., Ji, J., Yan, K., Ding, S., Sun, X., Wu, Y., Ji, R.: Aigi-holmes: Towards explainable and generalizable ai-generated image detection via multimodal large language models (2025), <https://arxiv.org/abs/2507.02664> 3
74. Zhuang, W., Chu, Q., Tan, Z., Liu, Q., Yuan, H., Miao, C., Luo, Z., Yu, N.: Uia-vit: Unsupervised inconsistency-aware method based on vision transformer for face forgery detection. ArXiv **abs/2210.12752** (2022), <https://api.semanticscholar.org/CorpusID:253098189> 3, 8, 9, 4
75. Zou, Z., Gong, B., Wang, L.: Attention to neural plagiarism: Diffusion models can plagiarize your copyrighted images! In: Proceedings of the IEEE/CVF International Conference on Computer Vision (ICCV). pp. 19546–19556 (October 2025) 13, 14

The Regularizing Power of Language-Training Deepfake Detectors

Supplementary Material

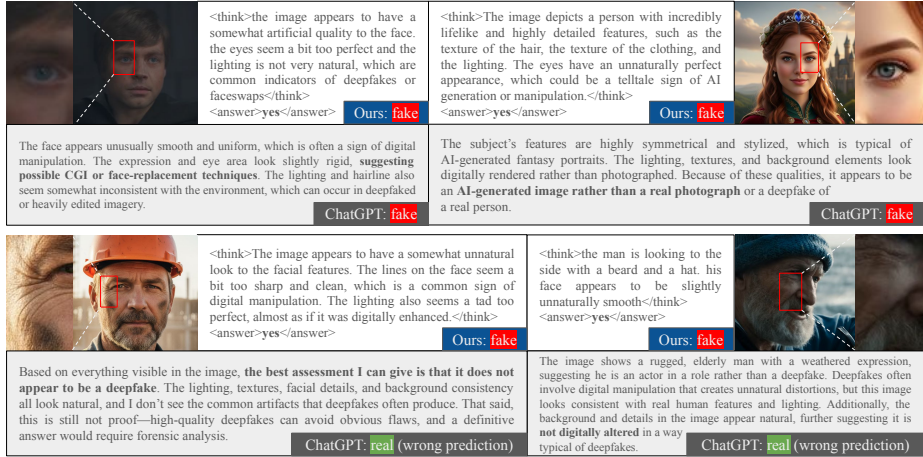


Fig. A: Samples from modern generators (all images are fake). Even though artifacts are very slight, our model can detect and describe them. In addition to two images from [17], we include two high-quality deepfakes from external sources: The first image is the famous Luke Skywalker Deepfake from The Mandalorian [16] (movie quality), and the last image is taken from the trailer video of Google’s Veo 3 [57], which presumably showcases Veo’s best outputs. We also provide explanations by ChatGPT [43] for comparison. Note that while ChatGPT generally focuses on global artifacts (lighting, textures, ...), our method points out very locally detailed artifacts.

Overview

This document provides additional information that could not be included in the main paper. First, we provide more qualitative examples of our method on modern SOTA generators and compare to ChatGPT (Sec. A). Then, we give a full comparison to previous works on legacy datasets in Sec. B and provide more qualitative comparisons to SOTA language-based deepfake detectors in Sec. C. Next, we provide details on the user study (Sec. D), computational requirements (Sec. E), reasoning (Sec. F), and method parameters (Sec. G) as well as more qualitative samples on DF40 [66] (Sec. H) and our difference to related work (Sec. I). Finally, in Sec. J, we provide some examples from related work on the usage of the term “(deep)fake”.

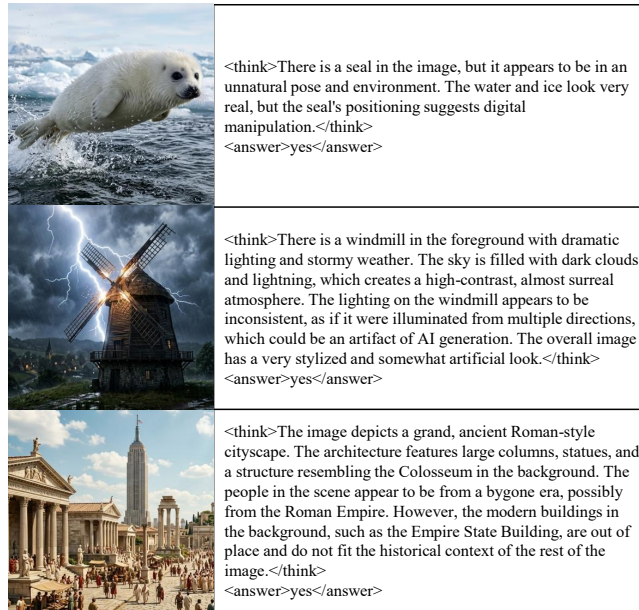


Fig. B: AIGI samples from Gemini 3 Flash [46]. All shown images are fake. Note how our model can integrate general real-world knowledge into its explanations.

A Samples from modern generators

We show some more examples from modern sources [10, 16, 17] in Fig. A. Since the first image is a Hollywood-grade deepfake, it is hard for a human to detect the fake. It is therefore notable that our model manages to recognize it, based on some slight inconsistency in the lighting. We attribute this to the SFT step, which effectively incorporates the specialized detector, allowing the detection of artifacts that are hard to spot – even for humans.

The second and third images both show very high image quality, but they appear overly perfect, with all lines (eyelashes, wrinkles, ...) appearing not random enough for a real photograph. Our model can point out these details, indicating that the RL finetuning is capable of teaching the model to capture fine artifacts without supervision.

Finally, the last image appears to have a very slight blur on the man’s cheek, which the model recognizes as a sign of a fake. We attribute this to the dual-encoder architecture and alignment: recognizing the small detail while being able to differentiate it from other types of blur, such as the blurry background and then describing it using the general vision features. These images show the generalization ability of our model, even to very high-quality fakes.

When comparing with explanations generated by ChatGPT [43], we observe that its explanations are relatively global (e.g., lighting, textures, ...), whereas our model can precisely pinpoint artifact areas. Furthermore, in two cases, Chat-

GPT does not detect the deepfake. This shows that for very high-quality deepfakes, finetuning is necessary, even when compared with very large commercial language models.

In Fig. B, we show some examples of the generalization capabilities of our model trained on SID-Set [26]. The first image shows a seal jumping out of the water, which would not be uncommon for a dolphin, but is not something seals do, which our model recognizes. This shows that, despite being trained on SID-Set, which includes only one generator (so learning its specific artifacts is possible), our model still incorporates external knowledge, enabling it to also generalize to images from different generators.

The second image shows lightning behind an old windmill. Still, the windmill is lit up from the front, which our model recognizes as a sign for AI generation. This exemplifies that our model can learn physical inconsistencies without direct supervision, underscoring the inherent capabilities of MLLMs due to their vast pretraining and multi-modal alignment.

Finally, in the last image, we test our model’s general knowledge. We generate an image of ancient Rome, but include the Empire State Building in the background. Our model recognizes the fact that this combination should not exist and therefore flags the image as fake. We can, therefore, observe that our model prefers high-level semantic inconsistencies over low-level generator-specific ones.

These examples show that while our model was mainly developed for deepfakes of faces, it works equally well on general images. Furthermore, we see that it effectively learns to incorporate high-level artifacts and explain them correctly without the need for full supervision during training.

B Comparison on legacy datasets

Here, we show a full comparative table with previous SOTA methods on the old SOTA datasets (Tab. A); numbers are directly taken from cited works. We see that our method performs best on CDFv2 [36], which is the most commonly used benchmark dataset. On the other two datasets, it performs similarly to the top methods, indicating that our model obtains comparable performance despite not having been specifically tuned for these datasets. Also, it is known that DFDC [13] and DFDCP [14] include low-quality images, and specifically designing a model for these low-quality conditions can be very helpful [23]. Since we aim for more modern datasets and explanations, we do not specifically tune our method for such circumstances and still achieve comparable performance. Also, note that it has been shown [66] that performance on these older datasets does not generalize well to more modern fakes, so we only include this comparison for completeness. The main indicator of performance should be newer methods, as described in Sec. 5.2.

Table A: Comparison on legacy datasets. Best values are highlighted in **bold**, second best values are underlined. Our method performs comparably to previous work, even on these older datasets for which the compared methods were specifically designed.

	Model	CDFv2	DFDCP	DFDC
Binary detectors	Xception [42, 48]	61.18%	69.90%	-
	EfficientNet-B4 [53, 63]	74.87%	72.83%	69.55%
	FaceXRay+BI [34]	79.50%	80.92%	65.50%
	RECCE [4]	68.71%	-	69.06%
	SPSL [37]	76.88%	74.08%	70.40%
	UIA-ViT [74]	82.41%	75.80%	-
	SeeABLE [33]	78.30%	86.30%	75.90%
	UCF [67]	75.27%	75.94%	71.91%
	Controllable GS [20]	84.97%	81.65%	-
	LSDA [64]	83.00%	81.50%	73.60%
	SBI [50]	93.18%	86.15%	72.42%
	LAA [42]	95.40%	86.94%	71.70%
	PMM [23]	91.53%	93.15%	75.21%
	Effort [65]	<u>95.60%</u>	90.90%	84.20%
	FakeSTormer [41]	92.40%	90.00%	74.6%
Language Detectors	BLIP-TI-Xcep. [48, 70]	62.41%	-	-
	BLIP-TI-RECCE [4, 70]	70.21%	-	-
	BLIP-TI-HiFi [18, 70]	71.00%	-	-
	BLIP-TI-SBI [50, 70]	93.98%	-	-
	VL-FFD [51]	84.80%	84.74%	-
	UCLVLM [69]	94.71%	<u>91.81%</u>	79.12%
	M2F2 [19]	95.10%	87.80%	-
	Ours	95.75%	90.29%	<u>82.75%</u>

C Comparison to SOTA language detectors

To compare to previous works [2, 19, 51, 69] in terms of explanation quality, we show examples in Fig. C. For the deepfake detection papers, we take images directly from the respective paper, therefore using the cases that the authors considered best to showcase their models’ performance. Despite being trained without full supervision, our explanations are similar or better, as our model can, for example, highlight blending boundaries, which are (if present) a reliable sign of a deepfake. The baseline Qwen [2] model does not find meaningful features as it is trained for general image recognition, showing that finetuning is necessary. M2F2 [19] provides comparable explanations to ours. However, they are limited to an annotated dataset and cannot easily be generalized to new data. VL-FFD [51] gives descriptions, which, while linguistically high quality, are not clear signs of deepfakes (like a mouth being abnormal in shape), and some explanations also do not match the image contents. Finally, UCLVLM [69] only provides very short descriptions, which are limited to the location of the artifact, which is generally “at the center of the image”. We therefore consider our explanations

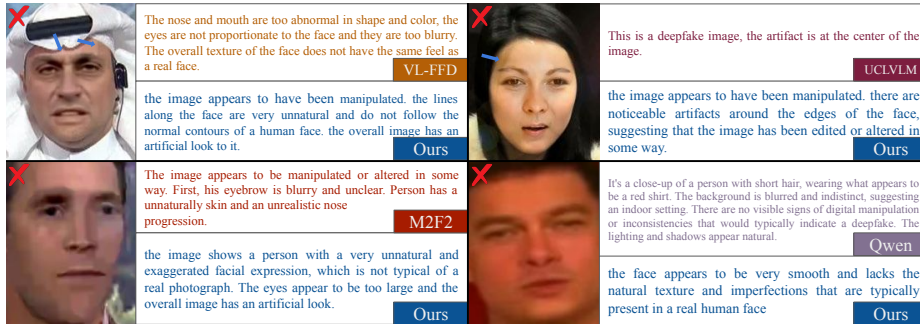


Fig. C: Comparison of our model to previous work (VL-FFD [51], UCLVLM [69], M2F2 [19] and a baseline Qwen [2]). We use the images and descriptions provided in the respective papers (except for Qwen) for a best-case scenario for the compared methods. Still, our model gives more useful answers, *e.g.* providing information about “unnatural lines” (manually marked with arrows in the figure) where applicable. All shown images are fake.

to be on par or better than the previous state-of-the-art, while only requiring binary labels for training instead of relying on supervision.

In Fig. D, we show more comparisons to previous language-based deepfake detectors. All images and texts are taken from the respective papers [19, 51, 69]. Our method performs comparably or better than related works, despite not having used supervision during training.

D User study details

For the user study, we asked three experts in the field of computer vision to judge the quality of our descriptions. Each participant was shown ten images and descriptions from DD-VQA [70] and ten from our method, in random order. Users were asked to rate the descriptions on a scale from 1 (bad) to 5 (good). From these values, we calculate the mean and standard deviation.

Given the small sample size, we verify the validity of our results using the bootstrap method [15]. We intend to show that our results are close to human labels, more specifically, that our mean opinion score is within one standard deviation of the reference mean opinion score.

We resample the results from the user study 1,000,000 times with replacement. For our method and the reference (human-labeled) data, we then calculate the mean μ_{ours}, μ_{ref} and standard deviation $\sigma_{ours}, \sigma_{ref}$. For the hardest test conditions, we set $\sigma = \min\{\sigma_{ours}, \sigma_{ref}\}$, so our score needs to be within the smaller of the two standard deviations. We then calculate the probability of $\mu_{ref} < \mu_{ours} + \sigma$. We find that probability to be 0.988. So the number of samples is sufficient to support the claim that our results are reasonably close (*i.e.* less than one σ) from human labels. We also test for $\mu_{ref} < \mu_{ours} + \sigma/2$ and find a



Fig. D: More comparisons to SOTA language-based deepfake detectors. We compare **our model** to previous work (**VL-FFD** [51], **UCLVLM** [69], **M2F2** [19]), using images directly from the respective papers. ✖: deepfake, ✓: real image.

Table B: Computational requirements. RL training requires significantly more FLOPs because of multiple autoregressive generations per input image.

Mode	training	Param.	trainable	TFLOPs
SFT	✓	8.6B	17M	16.8
SFT	✖	8.6B	-	5.6
RL	✓	8.7B	107M	178
RL	✖	8.7B	-	26.2

probability of 0.767, so we are likely even within half a standard deviation. On average, we find a distance of $0.34 \cdot \sigma$ between the mean opinion scores.

This shows that the quality of our explanations is roughly comparable to human annotations. The full set of images used is shown in Fig. E, to allow the reader to judge for themselves. We selected images for which the classification decision was taken correctly, as we only intend to measure the explanation quality of our method and not its detection performance, for which we have strong quantitative experiments.

E Computational requirements

Given that our model utilizes a large language model, it requires significantly more computational resources compared to more lightweight binary detectors. The computational cost for different configurations of our model is shown in Tab. B. The difference in parameters between the SFT and RL versions stems


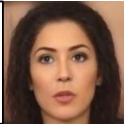

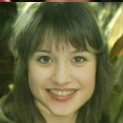
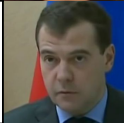




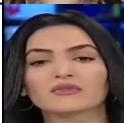
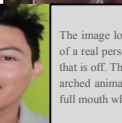

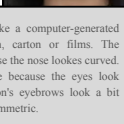
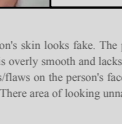

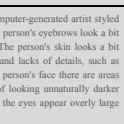
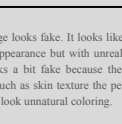

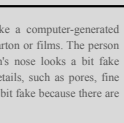
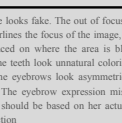
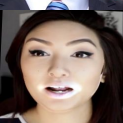
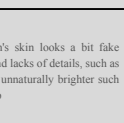
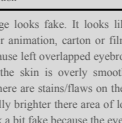
	There are no visible indicators in the image that suggest it is a deepfake. The person's appearance, including their hair and facial features, appears natural and consistent with what one would expect to see in a real photograph.		the image shows a person with dark hair and a light complexion. the features appear to be slightly exaggerated, which is a common characteristic of deepfakes		the woman's face appears to have an unreal quality, with a slight distortion that is not typical of a natural photo. the lighting also seems a bit too perfect and uniform
	the image appears to have an unnaturally perfect and sterile appearance. the woman's face looks too symmetrical and her skin has an unnaturally even tone, which are common indicators of digital manipulation		There are no visible indicators in the image that suggest it is a deepfake. The man appears to be a real person, and there are no unusual or suspicious elements that would typically be used to create a deepfake.		the woman's face appears to have a slightly unnatural sheen, and the edges of her features are not as sharply defined as they should be. These are common signs of digital manipulation.
	the woman's face appears somewhat unnatural, with an uncanny quality to it. the eyes seem slightly too prominently placed and the skin has a uniform tone that isn't entirely natural		the woman's face appears to have an unreal quality, with a slight distortion that is not typical of a natural photo. the lighting also seems a bit too perfect and uniform		the man's face appears to have an unusual glow, and the features seem to be slightly too smooth. these are subtle clues that suggest the image might be a deepfake or a faceswap.
	the man in the image appears to have an unnaturally idealized appearance. the lighting is very even and the colors are too vibrant, which is not typical of a real photograph. these are strong indicators that the image has been manipulated.		The person's skin looks real. The person has naturally smooth illuminated skin		The image looks real. Image has the look and feel of a real person. The mind is not noticing anything that is off. The person has smooth illuminated skin, arched animated eyebrows, oval eyes, broad nose, full mouth white teeth aligned teeth.
	The image looks fake. It looks like a computer-generated artist styled image for animation, cartoon or films. The person's nose looks very fake because the nose looks curved. The person's eyes look a bit fake because the eyes look unnaturally asymmetric. The person's eyebrows look a bit fake because the eyebrows look asymmetric.		The person's skin looks fake. The person's skin looks a bit fake because the skin is overly smooth and lacks of details, such as skin texture. There are stains/flaws on the person's face. There are areas looking unnaturally brighter. There area of looking unnaturally darker		The image looks fake. It looks like an ai-generated image although with human appearance but with unrealistic texture or lighting. The person's skin looks a bit fake because the skin is overly smooth and lacks of details, such as skin texture. the person's mouth looks very fake because the teeth look unnatural coloring.
	The image looks fake. It looks like a computer-generated artist styled image for animation, cartoon or films. The person's skin looks a bit fake because the skin is overly smooth and lacks of details, such as skin texture. there are stains/flaws on the person's face there are areas looking unnaturally brighter there area of looking unnaturally darker the person's eyes look a bit fake because the eyes appear overly large to the face.		The image looks fake. The out of focus on all of the facial details the person has blurry hairlines the focus of the image, some of the proportions and placement, it seems placed on where the area is blurry the person's mouth looks very fake because the teeth look unnatural coloring. The person's eyebrows look very fake because the eyebrows look asymmetric. The eyebrows do not match the face's structure. The eyebrow expression misplaces the natural position of where the eyebrows should be based on her actual expression, they are not moving in the right direction		The image looks fake. It looks like a computer-generated artist styled image for animation, cartoon or films. The person's skin looks a bit fake because the skin is overly smooth and lacks of details, such as skin texture. there are stains/flaws on the person's face there are areas looking unnaturally brighter there area of looking unnaturally darker the person's eyes look a bit fake because the eyes appear overly large to the face.
	The image looks fake. It looks like a computer-generated artist styled image for animation, cartoon or films. The person has mismatched bangs. The person's nose looks a bit fake because the nose lacks of subtle details, such as pores, fine lines. The person's eyebrows look a bit fake because there are boundaries between eyebrows.		The image looks fake. The person's skin looks a bit fake because the skin is overly smooth and lacks of details, such as skin texture. there are areas looking unnaturally brighter such as whole facial area. Heavy make up		The image looks fake. It looks like a computer-generated artist styled image for animation, cartoon or films. The person's skin looks a bit fake because the skin is overly smooth and lacks of details, such as skin texture. there are stains/flaws on the person's face there are areas looking unnaturally brighter there area of looking unnaturally darker the person's eyes look a bit fake because the eyes appear overly large to the face.
	The image looks fake. The person's skin looks a bit fake because the skin is overly smooth and lacks of details, such as skin texture. there are areas looking unnaturally brighter such as whole facial area. Heavy make up				

Fig.E: Images and captions used in our user study. The first ten captions (white) are from our method, the remaining ten (grey) are human annotations from the DD-VQA dataset [70]. All final decisions are correct, in order to only compare explanation quality.

from the use of different-sized LoRA adapters (ranks 4 and 32, respectively). We also see that the number of FLOPs during inference in RL mode (*i.e.* when generating descriptions) is significantly lower than during training. This happens because during training, we need to sample multiple sequences to have a group of answers to compare to. We use $G = 4$ samples per group. Since the answer length is stochastic, the number of FLOPs in RL mode is not fixed. The shown values are averages of 30 groups.

During training, backward passes and parameter updates have to be calculated, which is already included in the numbers.

F Reverse Reasoning

To show that the performance improvement in the RL stage actually stems from reasoning (and thereby a preference for high-level features), we conduct another experiment with reverse reasoning. That is, we use the same experimental settings as before, but the requested output format is now reversed (*i.e.* `<answer>[a-z]+</answer>\n<think>.*</think>`, prompts are phrased accordingly). While this setup still uses RL, it does not enforce the usage of describable artifacts, because by the time they would be needed, the decision is already taken. Since only the decision is supervised, the explanation is free to hallucinate. When testing, we measure a performance of 92.93%, which is even lower than the SFT-only result of 93.34%. This shows that not RL in general improves detection performance, but the specific enforcement of generalizable and describable artifacts. Note that, as with all quantitative experiments, no reasoning was generated during testing, so performance differences are restricted to feature selection as the answer pattern was not used during testing.

G Method details

For each input image, we generate a group of $G = 4$ sample answers using a temperature of $\tau = 1$. Limited by our GPUs' 48GB of VRAM, we generate a maximum answer length of 120 new tokens. The model learns to generate fewer than the set number of new tokens, as running into the generation limit will prevent it from completing the format requirements (*i.e.* finishing with `</answer>`). Furthermore, we randomly select one out of five possible prompts for each input image in order to avoid overfitting to a specific prompt. We leave the curation of a dataset of potential prompts for further improved diversity to future work.

During testing, we align with the common protocols [42, 50, 66] of providing video-level statistics for the legacy datasets and frame-level statistics for DF40.

Table C provides more detailed AUCs for some baseline configs from the ablation.

G.1 Meaning of α

During training, we use $\alpha = 0.01$ in order for the format reward to dominate correctness, which aids stability in the early stages of training. Here we prove

Table C: Baselines on DF40 splits, in line with Tab. 1. These are also covered in the ablation, but we provide additional detailed AUCs on these relevant baseline configurations.

Model	FS↑	FR↑	EFS↑
Qwen	68.17%	83.92%	76.98%
Reasoning inference	80.84%	79.37%	84.69%
SFT / binary alignment	93.90%	90.39%	95.73%
Ours	93.43%	92.38%	96.04%

that once the format is properly followed (*i.e.* $r_i^f = r_j^f \forall i, j \in \mathcal{G}$), the choice of α becomes irrelevant.

Proof. Let $r_i^f = r_j^f \forall i, j \in \mathcal{G}$. Then A_g is given as follows:

$$A_g = \frac{r_g - \text{mean}_g(r)}{\text{std}_g(r)} = \frac{r_g - \frac{1}{G} \sum_{j=1}^G r_g}{\sqrt{\frac{1}{G-1} \sum_{j=1}^G \left(r_j - \frac{1}{G} \sum_{i=1}^G r_i \right)^2}} \quad (9)$$

$$= \frac{r_g^f + \alpha r_g^c - \frac{1}{G} \sum_{j=1}^G \left(r_j^f + \alpha r_j^c \right)}{\sqrt{\frac{1}{G-1} \sum_{j=1}^G \left(r_j^f + \alpha r_j^c - \frac{1}{G} \sum_{i=1}^G \left(r_i^f + \alpha r_i^c \right) \right)^2}} \quad (10)$$

$$= \frac{r^f + \alpha r_g^c - \frac{1}{G} \sum_{j=1}^G \left(r^f + \alpha r_j^c \right)}{\sqrt{\frac{1}{G-1} \sum_{j=1}^G \left(r^f + \alpha r_j^c - \frac{1}{G} \sum_{i=1}^G \left(r^f + \alpha r_i^c \right) \right)^2}} \quad (11)$$

$$= \frac{r^f + \alpha r_g^c - \frac{1}{G} \sum_{j=1}^G r^f + \frac{1}{G} \sum_{j=1}^G \alpha r_j^c}{\sqrt{\frac{1}{G-1} \sum_{j=1}^G \left(r^f + \alpha r_j^c - \frac{1}{G} \sum_{i=1}^G r^f + \frac{1}{G} \sum_{j=1}^G \alpha r_i^c \right)^2}} \quad (12)$$

$$= \frac{r^f + \alpha r_g^c - r^f + \alpha \frac{1}{G} \sum_{j=1}^G r_j^c}{\sqrt{\frac{1}{G-1} \sum_{j=1}^G \left(r^f + \alpha r_j^c - r^f + \alpha \frac{1}{G} \sum_{j=1}^G r_i^c \right)^2}} \quad (13)$$

$$= \frac{\alpha \left(r_g^c + \frac{1}{G} \sum_{j=1}^G r_j^c \right)}{\sqrt{\frac{1}{G-1} \sum_{j=1}^G \left(\alpha \left(r_j^c + \frac{1}{G} \sum_{j=1}^G r_i^c \right) \right)^2}} \quad (14)$$

$$= \frac{\alpha \left(r_g^c + \frac{1}{G} \sum_{j=1}^G r_j^c \right)}{\sqrt{\frac{1}{G-1} \sum_{j=1}^G \alpha^2 \left(r_j^c + \frac{1}{G} \sum_{j=1}^G r_i^c \right)^2}} \quad (15)$$

$$= \frac{\alpha \left(r_g^c + \frac{1}{G} \sum_{j=1}^G r_j^c \right)}{\sqrt{\alpha^2 \frac{1}{G-1} \sum_{j=1}^G \left(r_j^c + \frac{1}{G} \sum_{j=1}^G r_i^c \right)^2}} \quad (16)$$

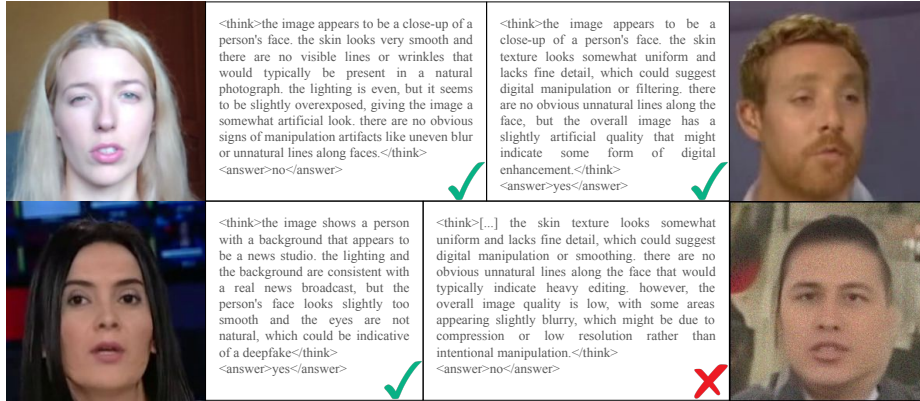


Fig. F: Sample explanations based on DF40 images. Note that even in the case of a wrong final decision, the explanation can still be helpful to the user. ✖: wrong decision, ✔: correct decision.

$$\alpha \frac{\left(r_g^c + \frac{1}{G} \sum_{j=1}^G r_j^c \right)}{\sqrt{\frac{1}{G-1} \sum_{j=1}^G \left(r_j^c + \frac{1}{G} \sum_{j=1}^G r_i^c \right)^2}} \quad (17)$$

$$= \frac{r_g^c + \frac{1}{G} \sum_{j=1}^G r_j^c}{\sqrt{\frac{1}{G-1} \sum_{j=1}^G \left(r_j^c + \frac{1}{G} \sum_{j=1}^G r_i^c \right)^2}} = \frac{r_g^c - \text{mean}_g(r^c)}{\text{std}_g(r^c)} \quad (18)$$

Which does not depend on α anymore.

H Additional DF40 samples

In Fig. F, we show additional sample explanations based on the DF40 [66] dataset. We include a failure case to demonstrate that even an incorrect detection can provide meaningful insights for the user. In that case, the model notices uniform skin texture, which can be a sign of a fake, but given the lack of blending boundaries *etc.* it finally decides “real”. Such an output still provides the user with helpful information, allowing them to decide for themselves if these signs are sufficient for considering the image fake. Note that our model provides arguments for both sides in multiple cases. In addition to enhancing interpretability, this also shows that our model does not simply sample explanations that correlate with the answer, but actually examines the image.

I Details on related work

Table D shows a comparison of our method to related work in terms of its requirements for training. Our model and RAIDX are the only ones to be able

Table D: Details on related work showing how our model differs from other LLM-based deepfake detectors. *Language Supervision* refers to a supervised stage during training, regardless of whether the supervision comes from dataset annotation or some heuristic. *@inference* refers to using reasoning at inference, rather than only for regularization. (✖) refers to using reasoning on some samples and not on others, n/a refers to a separate detection head, so reasoning is independent from detection.

Name	Language Supervision	Faketype	Retrieval	Post-hoc	@inference
VL-FFD [51]	✖	Faces	-	✖	n/a
UCLVLM [69]	✖	Faces	-	✖	n/a
M2F2 [19]	✖	Faces	-	✖	n/a
RAIDX [35]	-	fully synth.	✖	-	✖
Veritas [52]	✖	fully synth.	-	-	✖
ThinkFake [25]	✖	fully-synth.	-	-	(✖)
So-Fake [27]	✖	All	-	-	✖
Ivy-Fake [28]	✖	All	-	-	✖
Ours	-	All	-	-	-

to work without language supervision. However, RAIDX requires retrieval and only works on fully-synthetic images, making it significantly less flexible.

J On the definition of fake

The definition of deepfake remains fundamentally ambiguous. The prevailing view frames an image as fake primarily when it is AI-generated. Under this perspective, an untouched photograph is unquestionably real, while face swaps or fully synthetic images are fake. Yet such a dichotomy collapses under closer scrutiny. For example, is a background change, routine in videoconferencing, considered fake? And if so, by what standard?

Our observations underscore this ambiguity. Using an image from [58] (see Fig. G), we compare background removal and replacement. A plain white background is often judged as real by most human observers, and our proposed model, which also joins the conclusion from commercialized GPT. Yet this perception of “realness” is semantically questionable: the removal

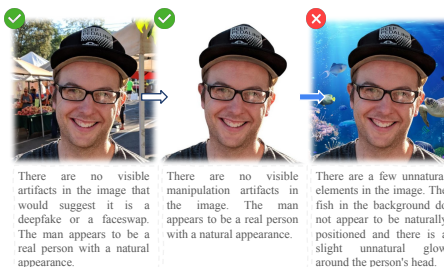


Fig. G: What is a fake? There exists a grey area between fakes and real images, *e.g.* in the case of background removal. Our exemplary testing indicates that our model, in this case, bases its decision on the practical realism of the content of the image. We only print our model’s descriptions, omitting format and decision.

may be AI-assisted, and lighting inconsistencies undermine physical plausibility, *i.e.* the lighting on the face suggests that a pure white background is not possible. By contrast, placing the same person underwater immediately feels fake – not because of the editing tool, but because the scene could not have occurred.

These examples expose a deeper tension: Should fakes be defined by the process (AI-generated) or the outcome (depicting events that never occurred)? Current definitions conflate these criteria, resulting in unstable and context-dependent judgments. This highlights the need to clarify and standardize what we mean by “fake” in the first place.

Here we compile some examples from related work to show that the definition of “fake” is by no means as clear as it may seem. While the term “deepfake” might indicate the usage of some “deep model”, this does not always need to be the case. The main training dataset FaceForensics++ [48] includes FaceSwaps [32], which do not use deep generative methods. Furthermore, some works [34, 50] create pseudo-fakes, which directly blend two faces, without an intermediate generative step. While these are *pseudo*-fakes, they are used to train detectors, indicating that they should be considered fake. Specifically [50] introduces inconsistencies in sharpness and color, between face and background, indicating that local manipulations are considered fake. Several works [23, 42, 63] consider such manipulations on the full image to not constitute a fake. Even changes made by deep models are not necessarily considered fake, as *e.g.* superresolution is not considered deepfake in [66], but only described as creating similar generative artifacts.

Finally, for the case of background removal, the FaceForensics++ dataset [48] includes several “real” videos, taken from TV broadcasts with replaced backgrounds (probably using a green-screen).

This overview is not meant to give a final answer to what should be fake, but to spark a discussion, which may lead to a standardized definition of the term “(deep)fake”.